British Journal of Pharmacology (2007) 151, 1049–1060

www.brjpharmacol.org

RESEARCH PAPER

Blockade of gap junction coupling by glycyrrhetinic acids in guinea pig cochlear artery: A whole-cell voltage- and current-clamp study

B-C Guan[1], J-Q Si[1,2] and Z-G Jiang[1]

[1]*Department of Otolaryngology, Oregon Hearing Research Center, Oregon Health and Science University, Portland, OR, USA and* [2]*Department of Physiology, Shihezi University Medical College, Shihezi, Xinjiang, PR China*

Background and purpose: Glycyrrhetinic acids (GAs) are widely used as gap junction blockers, but their efficacy and side effects have not been well determined.
Experimental approach: Whole-cell electrical recordings were made from vascular smooth muscle cells (VSMCs) embedded in or dissociated from, guinea pig cochlear artery segments.
Key results: 18β- & 18α-GA concentration-dependently increased membrane input resistance (R_{in}) of *in situ* VSMCs, with a maximal input conductance ($G_{in} = 1/R_{in}$) reduction of 92% & 77% and IC_{50} of 2.0 & 4.4 μM, respectively. 18βGA (30 μM) resulted in a R_{in} of 2.2 GΩ and C_{in} of 12 pF, comparable to those of freshly dissociated VSMCs (3.1 GΩ & 6.1 pF). The GAs ($\geq$30 μM) caused a depolarization in VSMCs *in situ*. In dispersed VSMCs, they both inhibited delayed rectifiers; 18βGA also activated a non-selective cation conductance while 18αGA inactivated a voltage-independent K^+-conductance. ACh induced an outward current in VSMCs *in situ* at –40 mV, with a positive slope *I*/*V* relation and a reversal potential near E_K. The ACh-induced current was attenuated by 18β- & 18αGA with an IC_{50} of 4.3 & 7.8 μM, respectively.
Conclusions and Implications: 18βGA blocked the vascular gap junctions, achieving a complete electrical isolation of the recorded VSMC at $\geq$30 μM while causing a mild depolarization by a complex conductance alteration. 18βGA suppressed the ACh-induced current in VSMC by blocking the myoendothelial gap junction and by a non-junctional action. 18αGA at 30-100 μM failed to fully block the gap junctions while exerting side actions.
British Journal of Pharmacology (2007) **151,** 1049–1060; doi:10.1038/sj.bjp.0707244; published online 18 June 2007

Keywords: arteriole; gap junction; EDHF; acetylcholine; membrane input conductance; vascular; cochlea

Abbreviations: 4AP, 4-aminopyridine; C_{in}, membrane input capacitance; EC, endothelial cell; EDHF, endothelium-derived hyperpolarizing factor; EGTA, ethylene glycol-*bis* [β-aminoethylether] *N*,*N*′,*N*′-tetraacetic acid; E_K, potassium equilibrium potential; GA, glycyrrhetinic acid; I_{cat}, cation current; HC, holding current; HP, holding potential; K_{DR}, delayed rectifier potassium channel; K_{ir}, inward rectifier potassium channel; K_{Ca}, calcium-activated potassium channel; K_V, voltage-dependent potassium channel; MA, mesenteric arteriole; OD, outside diameter; R_a, access resistance; R_{in}, membrane input resistance; SMA, spiral modiolar artery; V_{rev}, reversal potential; TEA, tetraethylammonium; VSMC, vascular smooth muscle cell

Introduction

Gap junction coupling permits intercellular electrical and certain chemical communications, and thus plays an important role in cellular homeostasis, development and normal function of many organs, including the inner ear (Sabag *et al*., 2005). It is known that several forms of familial hearing loss result from mutations in connexins, a family of transmembrane proteins that form the gap junction channels (Kikuchi *et al*., 2000; Sabag *et al*., 2005; Palmada *et al*., 2006). Gap junctions also play a key role in the structure, physiology and pathology of blood vessels (Figueroa *et al*., 2004; Griffith, 2004; Sandow, 2004), including the inner ear artery (Jiang *et al*., 2005).

For instance, a number of endogenous vasoactive substances, such as acetylcholine, substance P and bradykinin cause muscular hyperpolarization and vasodilation via endothelium-derived hyperpolarizing factor (EDHF); the nature of EDHF has been an intensive research topic in the cardiovascular field in the last two decades (Busse *et al*., 2002; Griffith, 2004; Segal, 2005). Yamamoto *et al*. (2001) claimed

Correspondence: Professor Z-G Jiang, OHRC/Otolaryngology, Oregon Hearing Research Center, Oregon Health and Science University, 3181 SW Sam Jackson Park Road, Portland, OR 97239, USA.
E-mail: Jiangz@ohsu.edu
Received 29 December 2006; revised 12 February 2007; accepted 16 February 2007; published online 18 June 2007; corrected 30 July 2007

that myoendothelial gap junction coupling is solely responsible for the transmission of a primary hyperpolarization from endothelium to the muscle cells in guinea pig mesenteric arterioles (MAs), whereas others identified the EDHF as K^+, nitric oxide (NO), prostaglandins and cytochrome P450 products epoxyeicosatrienoic acids in various vascular preparations (Busse *et al*., 2002). These EDHF constituents may each play a variable role in different vascular beds, but the gap junction appears to be the major and universal mechanism (Griffith, 2004; Sandow, 2004).

To identify the role of gap junction electrical coupling, many studies, including ours (Jiang *et al*., 2001, 2005), used gap junction blocker(s) such as heptanol, octanol, 18α-glycyrrhetinic acid (18αGA), 18β-glycyrrhetinic acid (18βGA) or carbenoxolone. Heptanol, octanol and carbenoxolone have been found to be ineffective on gap junctions in several arteries (Yamamoto *et al*., 1998; Coleman *et al*., 2001). The compounds 18αGA and 18βGA have been used more widely in blocking vascular gap junctions (Coleman *et al*., 2001; Yamamoto *et al*., 2001; Jiang *et al*., 2005) but their efficacy and specificity have not been well determined. This has stimulated controversy in recent literature; for instance, Coleman *et al*. (2001) found that in an intracellular recording study, the GA compounds exerted only a weak block on the gap junctions in guinea pig submucosal arterioles and had strong non-specific actions, so they claimed that the compounds are useless in testing gap junction involvement in EDHF-attributed responses. On the other hand, several whole-cell recording studies demonstrated excellent blocking action of 18βGA (20–30 μM) on electrical coupling in guinea pig MAs (Yamamoto *et al*., 1998, 1999, 2001). Moreover, using sharp electrode intracellular recording, we found that 18βGA (25–30 μM) almost completely blocked electrical transmission of acetylcholine hyperpolarization from the endothelial cell (EC) to the vascular smooth muscle cell (VSMC) and the transmission of high K^+-induced hyperpolarization from the VSMC to the EC (Jiang *et al*., 2005).

We analyzed two commonly used GA compounds regarding their efficacy of gap junction blocking action and their non-junctional membrane actions, using whole-cell recording techniques on the VSMC embedded in (*in situ*) and dispersed from cochlear spiral modiolar artery (SMA) segments. We found that both the GAs concentration-dependently blocked both myoendothelial and intramuscular electrical coupling, and 18βGA at $\geqslant$30 μM could achieve complete electrical isolation of the recorded VSMC. Some preliminary results have appeared as a meeting abstract (Guan *et al*., 2006).

Materials and methods

Preparation of segments of the SMA

All animal procedures were approved by the Institutional Animal Care and Use Committee of Oregon Health & Science University. Guinea pigs (250–450 g) were killed by exsanguination under general anesthesia induced by intramuscular injection of an anesthetic mixture (1 ml kg^{-1}) of ketamine (500 mg), xylazine (20 mg) and acepromazine (10 mg) in 8.5 ml water. Both bullae were quickly removed and transferred to a 100-mm Petri dish filled with Krebs solution composed of (mM): NaCl 125, KCl 5, $CaCl_2$ 1.6, $MgCl_2$ 1.2, NaH_2PO_4 1.2, $NaHCO_3$ 20 and glucose 7.5, and saturated with 95% O_2 and 5% CO_2 at 35°C (pH 7.4). The whole length of the SMA was dissected from the cochlea and cleaned of its surrounding connective tissue. Then a short segment of the vessel ($\sim$0.4 mm long, $\sim$40 μm OD (outside diameter), Figure 1 and Supplementary Figure S1) was transferred to a 35-mm glass-bottomed Petri dish filled with aerated normal external solution composed of (mM): NaCl 138, KCl 5, $CaCl_2$ 1.6, $MgCl_2$ 1.2, Na-4-(2-hydroxyethyl)-1-piperazineethanesulfonic acid (Na-HEPES) 5, HEPES 6, glucose 7.5, with pH 7.4 and osmolarity of 300 mOsm l^{-1}. The preparation was secured at the bottom of the dish by the weight of a platinum strip ($\sim 0.5 \times 2$ mm) on each end (Figure 1), and digested with collagenase A (0.75 mg ml^{-1}, Roche, Basel, Switzerland) dissolved in the normal external solution at 36°C for $\sim$20 min. After completely washing out the enzyme with the normal external solution, the vessel was further cleaned of its adventitial tissue in certain areas with fine tweezers under a stereoscope. Then, the Petri dish was placed onto the stage of an inverted microscope (Zeiss, Axiovert 35, Carl Zeiss, MicroImaging GmbH, Standort Göttingen, Germany) equipped with DIC function, video camera and micromanipulators (Siskiyou Design Instruments, MX7600R & MX10L, Grants Pass, Oregon, USA). The SMA segment and the electrode pipette were visualized with 10×20 magnification with DIC on (Figure 1).

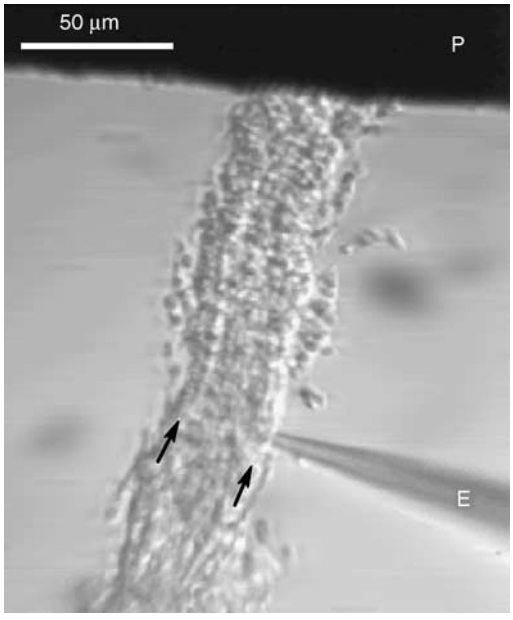

Figure 1 Microscopic view of whole-cell recording from *in situ* smooth muscle cells. The DIC micrograph shows a view of whole-cell recording of a smooth muscle cell embedded in a segment of SMA (300 μm long, and $\sim$40 μm OD) with an electrode pipette (E). The SMA segment was pre-digested with collagenase A (0.75 mg ml^{-1}) for 20 min at 36°C and manually cleaned of its adventitial connective tissue. The black stripe at the top is one of the two platinum chips (P) placed on each end of the SMA for stabilizing the vessel segment. Note that the two arrows denote a single layer of smooth muscle cell lining on each side of the vessel.

Dissociation of smooth muscle cells

Dissociated smooth muscle cells were prepared from the SMA and small mesenteric arteries of guinea pigs. The manually cleaned arteries were incubated for 20 min in a low Ca^{2+} buffer solution containing (mM): NaCl 142, KCl 5, $CaCl_2$ 0.05, $MgCl_2$ 1, Na-HEPES 4, HEPES 5 (pH 7.2) and glucose 7.5. Then the arteries were cut into segments (1 mm long) and digested for 20–25 min at 37°C with this buffer solution supplemented with papain 0.75 mg ml^{-1}, collagenase IA 1 mg ml^{-1}, bovine serum albumin 3.75 mg ml^{-1} and dithiothreitol 0.3 mg ml^{-1}. After centrifuging (67 *g* for 5 min) and replacing the supernatant with enzyme-free buffer three times, the preparation was triturated with a fire-polished Pasteur pipette. The cell-rich suspension was transferred to a 35 mm Petri dish with a coverslip-bottom coated by poly-L-lysine. Once the dispersed cells attached to the glass bottom, the dish was mounted on the stage of an inverted microscope (Zeiss, Axiovert 35) and perfused with normal extracellular solution (see above) for 20 min before whole-cell recording. The VSMC was identified by its characteristic spindle-shape (Supplementary Figure S2, also see Quinn and Beech, 1998; Bradley *et al*., 1999).

Tight-seal whole-cell recording

Using an Axopatch 200B amplifier (Axon Instruments Inc., Union City, CA, USA), conventional whole-cell recordings were performed on smooth muscle cells *in situ* and dissociated from the SMA. The specimen was continuously superfused with the normal external solution (0.2 ml min^{-1}) at room temperature (22–25°C). Recording pipettes were made of borosilicate glass capillaries with filament (OD 1.5 mm, ID 0.84 mm; World Precision Instruments, Sarasota, FL, USA) and pulled by a Sutter Instruments P-80 puller. The pipette was filled with an internal solution containing (mM): K-gluconate 130, NaCl 10, $CaCl_2$ 2.0, $MgCl_2$ 1.2, HEPES 10, EGTA 5 (118 nM free Ca^{2+}) and glucose 7.5, adjusted to pH 7.2 and to osmolarity 290 mOsm l^{-1}. The recording pipettes had a tip of $\sim$1 μm OD and a resistance of $\sim$5 MΩ. Pipette capacitance was well compensated, while membrane input capacitance (C_{in}) uncompensated to monitor access resistance (R_a) and membrane parameters online. The voltage clamping error introduced by the current (I) passing the access resistance was corrected offline according to the equation $V_m = V_C - IR_a$ (in which V_m is the actual clamping membrane voltage and V_c is the apparent command voltage), except where noted otherwise. Leak subtraction was done offline when appropriate. Membrane current or voltage signal was low-pass filtered at 5 or 10 kHz (−3 dB); data were recorded on a PC computer equipped with a Digidata 1322A AD-interface and pClamp 9.2 software (Axon Instruments Inc.) at a sampling interval of 10, 20 or 100 μs. A gap-free recording was simultaneously carried out by a Minidigi digitizer and Axoscope 9.2 software (Axon Instruments Inc.) at a sampling interval of 50 ms.

Drug application

Drugs were applied at room temperature by superfusion via an array of capillary inlets near the preparation in the dish. The solution flowing over the preparation could be switched quickly to one that contained a drug(s) or one of different ionic composition by shifting the inlets. Drugs used in this study included acetylcholine, 4-aminopyridine (4AP), tetraethylammonium (TEA), 18αGA (all from Sigma-Research Biochemicals Inc., St Louis, MO, USA), and 18βGA (MP Biomedicals, Irvine, CA, USA). The latter two compounds were dissolved in dimethylsulfoxide (DMSO) to a 0.1–100 mM stock solution before being further diluted with normal external solution to final concentrations ranging from 0.1 to 100 μM. A solution of 18αGA at 100 μM became saturated thus no higher concentrations could be tested.

Data analysis

Results are expressed as means ± s.e.m. Differences between mean values of IC_{50} were assessed by Student's *t*-test, after log transformation. Values of $P<0.05$ were taken as showing significant differences.

Results

General findings

Whole-cell recordings were made from *in situ* and dispersed VSMCs of the SMA from 104 guinea pigs. Some Supplementary data are from dispersed VSMCs of small MAs (OD <100 μm). Stable recording lasted from 5 min to 6 h on *in situ* cells, whereas only up to 2 h in dispersed VSMCs. The seal resistance usually reached 1–20 GΩ before rupture of the membrane. The mean holding current (HC_{-40}) of the *in situ* cells at a holding potential (HP) of −40 mV was negative (−69 ± 6.9 pA, $n=21$, Figures 2a and 3A), positive (62.6 ± 18.0 pA, $n=7$, Figure 3C) or near zero ($n=4$) when the recorded cell had resting membrane potential (RP) positive to, negative to or near the HP −40 mV, respectively. In zero current clamp mode, the *in situ* cells had a RP of −34 ± 1.7 mV ($n=54$, ranged from −19 to −63 mV), an input resistance (R_{in}) of $\sim$200 MΩ or an input conductance ($G_{in}=1/R_{in}$) of $\sim$6.7 nS (Table 1). The current transients during the voltage steps showed a time course that fitted poorly to a single-term exponential function (Figure 2d), but fitted well to a double or triple term exponential function (not shown). On the other hand, the dispersed VSMCs of the SMA had a RP of $\sim$−20 mV, a R_{in} of $\sim$3.0 GΩ and a C_{in} of $\sim$6.1 pF (Table 2) that always exhibited single exponential current transients, and a HC of −7.8 ± 1.0 pA ($n=52$, ranged from −23 to 2.2 pA) at −40 mV. The dispersed VSMCs of the MA had a similar RP and a slightly smaller R_{in} ($P>0.05$) but a significantly larger C_{in} (Table 2); the latter appeared to be owing to the noticeably larger size of the MA cells.

The I/V relation of whole-cell current of both *in situ* and dissociated cells showed an outward rectification, which was more marked in the latter, when the cell was depolarized beyond −30 mV (Figures 2a, b, 3 and 4a–c). The outward rectification was apparently owing to the delayed rectifier potassium current (K_{DR}), which was substantially inhibited by 10 mM TEA or 1 mM 4AP; the latter was less effective on the slow component (Figure 4), suggesting that the fast and slow K_{DR} components were largely mediated

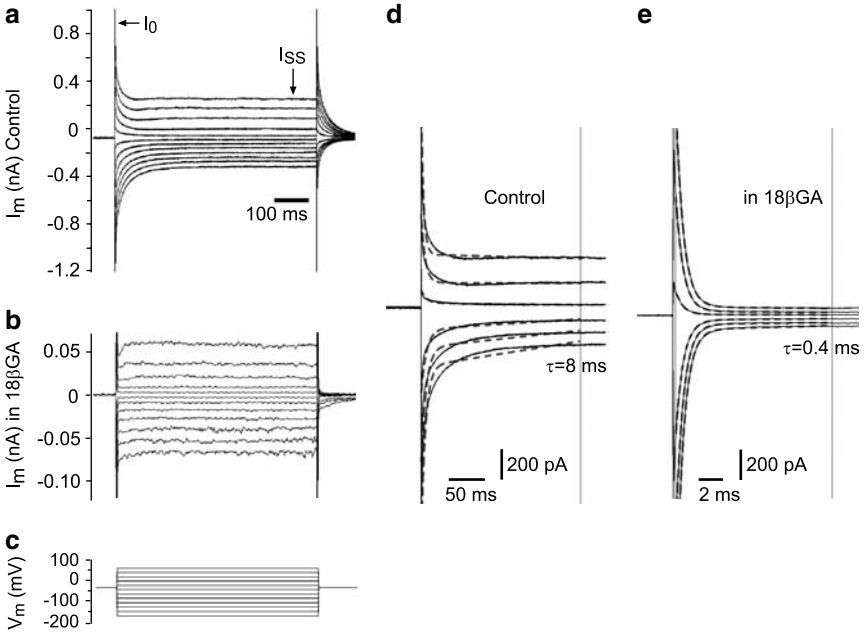

Figure 2 Electrical isolation of an *in situ* smooth muscle cell by 18βGA. (**a** and **b**) Membrane current (I_m) traces induced by voltage command steps (**c**) from the HP -40 mV in 20 mV increments before (**a**) and during (**b**) application of 30 μM 18βGA. Note that 18βGA caused a drastic reduction in the steady-state current (I_{ss}) or an input resistance increase from 0.58 to 4.57 GΩ. (**d** and **e**) Time scale expanded presentation of the initial part of **a** and **b**, respectively (traces alternatively omitted for clarity), showing that a single exponential function (dashed lines between two cursors) fitted well (overlapped) with the current transients (solid thin lines) in (**e**) ($r \geqslant 0.99$), but relatively poor ($r \leqslant 0.90$) in (**d**). With the single exponential fit, electrical parameters were computed according to the four equations (Armstrong and Gilly, 1992; Lindau and Neher, 1988): (1) $R_a = V_s/I_0$, (2) $R_{in} = (V_s - R_a I_{ss})/I_{ss}$, (3) $I_t = (I_0 - I_{ss})e^{(-t/\tau)} + I_{ss}$, (4) $C_{in} = \tau(1/R_a + 1/R_{in})$; where V_s is the step voltage amplitude; I_0 is the amplitude of the initial peak at the voltage step onset; t is the time after voltage step onset and τ is the time constant resulting from single exponential (equation 3) fit to the current decay. The τ and C_{in} obtained from the fitting of the bottom trace in the control were 8 ms and 241 pF, respectively; whereas, those in 30 μM 18βGA, were 0.4 ms and 13 pF, respectively. A good fit ($r \geqslant 0.98$) to *D* required a triple-term exponential function, revealing three time constants as 18.7, 2.6 & 0.39 ms for the bottom trace (not shown).

by Ca^{2+} independent (K_V) and Ca^{2+}-activated (BK_{Ca}) voltage-dependent K^+ channels, respectively (Jackson, 2005). About half of the *in situ* cells showed a significant inward rectification when the cell was hyperpolarized beyond -60 mV (Figures 2b and 3B), but this was less frequently seen in dispersed VSMCs (15 of 51, data not shown). The inward rectification of *in situ* VSMCs was facilitated by high extracellular K^+ (50 mM) and blocked by 100 μM Ba^{2+} ($n = 3$, data not shown), indicating its mediation by an inward rectifier K^+ channel (K_{ir}; Jackson, 2005).

GAs block the electrical coupling of in situ *smooth muscle cells*

Application of 30 μM 18βGA caused a significant attenuation of the steady-state current induced by voltage steps from the HP of -40 mV (Figure 2) in cells *in situ*. Table 1 and Figures 2 and 3 show the effect of 30 μM 18βGA on the membrane input resistance and input conductance near -40 mV. The whole-cell current I/V plots constructed by step commands (Figure 3A and B) or by ramp command (Figure 3C and D) showed that the slope conductance was drastically reduced by 18βGA in almost the whole range of command (-140 to 40 mV). The 18βGA-induced net current (Figure 3D) showed an approximately linear I/V relation with a negative slope and a reversal potential only slightly negative (by 2.6 ± 0.6 mV, $P < 0.001$, $n = 23$) to the pre-drug RP (Figure 3A, C and D), suggesting that the conductance reduction was mainly the blockage of electrical coupling. This is because when the GAs blocked only the intercellular gap junction coupling, that is, blocked only the resting currents of surrounding cells, the reversal potential of GA-induced current should be the same as the pre-drug RP, assuming that the surrounding cells in the short SMA segment were largely of equal potential. Furthermore, in the presence of 30 μM 18βGA, the current decay became well fitted by a single-term exponential function (Figure 2e), and the input capacitance was thus estimated to be 12 ± 3.2 pF ($n = 7$).

All these effects became noticeable in less than 1 min of drug application and reached the maximum in 3–5 min, whereas the stock solvent DMSO (1/1000, the dilution used) had no such effects ($n = 3$). About 75% recovery of membrane conductance was reached after a 15–25 min wash with drug-free solution. In a single-term exponential fit, the time constant and input capacitance before 18βGA application were always significantly larger than those in 18βGA (Figure 2d and e). Considering that the voltage control over surrounding cells was poor in this condition, no further quantitative analysis was made.

The drastic increase in R_{in} or reduction in G_{in} by 18βGA resulted in membrane parameters of the *in situ* cells very close to those of the dispersed VSMCs (Table 2), suggesting that 18βGA electrically isolated the recorded cell by blocking

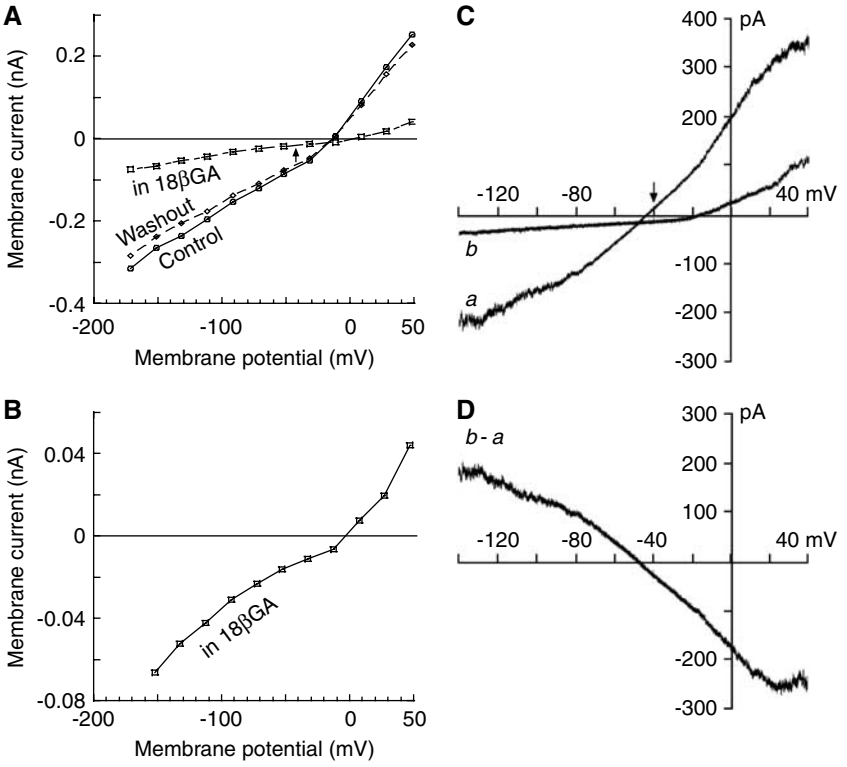

Figure 3 Effect of 18βGA on *in situ* whole-cell current *I/V* plots. (**A**) Steady-state *I/V* plots of the data of Figure 2a and b, showing that 18βGA caused an 8 mV depolarization in the RP (or zero current membrane potential) and a significant reduction of slope conductance in the full range of command potential. The arrow indicates an outward shift of the HC at -40 mV. (**B**) The same *I/V* curve of 'in 18βGA' in (**A**) but with the ordinate expanded, showing significant outward and inward rectifications. R_a error was not corrected in plots (**A** and **B**). (**C**) Ramp voltage command-constructed *I/V* curves of whole-cell currents before *(a)* and in the presence of 30 μM 18βGA *(b)* of another cell. Note the inward shift of the HC_{-40} (arrow) and a larger depolarization. (**D**) The *I/V* curve of 18βGA-induced net current *(b–a)* showed a linear relation between -80 and -20 mV with a negative slope of -3.6 nS and a reversal potential of -48 mV. Note that 18βGA-induced net current reversed near the pre-drug RP in both cells.

Table 1 Membrane actions of 18βGA and 18αGA on *in situ* VSMC

	18βGA (30 μM)			*18αGA (30 μM)*		
Membrane properties	*Control*	*In treatment*	*Change*	*Control*	*In treatment*	*Change*
Input resistance (MΩ)	184±30	2200±139** ($n=9$)	1401±255%	164±26	396±54** ($n=11$)	160±17%
Input conductance (nS)	6.7±1.0	0.47±0.036** ($n=9$)	−91±2.1%	9.4±2.9	3.3±0.69* ($n=11$)	−60±2.4%
Resting potential (mV)	−29±1.4	−19±1.8** ($n=12$)	10±1.8	−32±2.2	−26±1.0* ($n=10$)	5.8±1.8

*$P<0.05$, **$P<0.01$, paired *t*-test.

Table 2 Membrane properties of VSMCs dissociated from the SMA and from the MA

Groups of cells	*SMA*	*MA*
Input resistance near −40 mV (MΩ)	3071±199 ($n=55$)	2580±351 ($n=10$)
Resting potential (mV)	−19.6±1.21 ($n=23$)	−19.8±1.27 ($n=7$)
Input capacitance (pF)	6.13±0.19 ($n=55$)	13.3±0.42** ($n=10$)

**$P<0.01$, Student's *t*-test.

the gap junction coupling. However, the R_{in} or G_{in} measurement in 18βGA should also include its possible non-junctional membrane action indicated by the depolarization (Table 1), so the non-junctional membrane action was analyzed in dissociated VSMCs of the SMA below. The data indicated that 18βGA caused a 17.8% decrease in single cell R_{in} (Table 3). In other words, without this decrease, 18βGA would have increased the *in situ* cell R_{in} to a higher level (2.2 GΩ/(1–0.178) = 2.67 GΩ).

The blocking effect of 18βGA on electrical coupling was concentration dependent. An increase in R_{in} or a decrease in G_{in} by 18βGA was often detectable at a

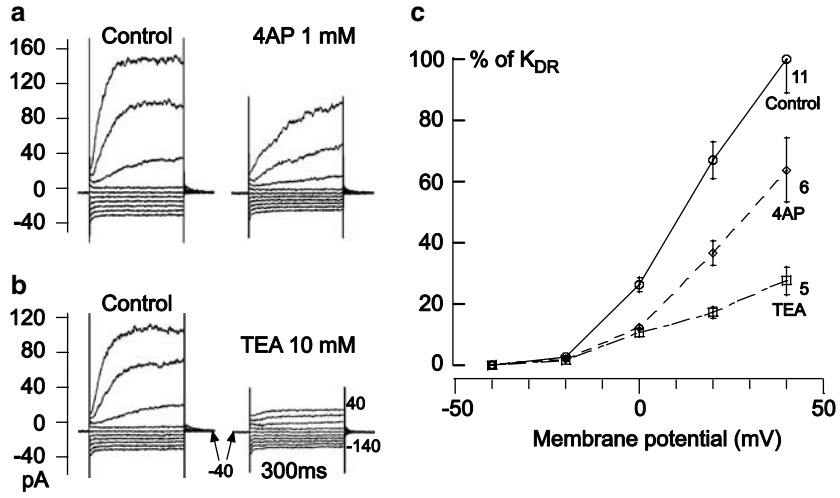

Figure 4 The delayed rectifier current (K_{DR}) of dissociated VSMCs of the SMA was sensitive to 4AP and TEA. (**a** and **b**) Sample recordings of whole-cell currents elicited by step commands (from HP of −40 to −140 and +40 mV in 20 mV increments). (**c**) Plots of leak-subtracted steady-state currents normalized to control values at 40 mV. Note that 1 mM 4AP caused an inhibition ($P<0.01$) similar to that of 10 mM TEA at −20 and 0 mV, but a significantly smaller inhibition than TEA at 20 and 40 mV ($P<0.05$). The K_{DR} suppression was largely reversible upon washout of the channel blockers, especially for TEA.

Table 3 Membrane actions of 18βGA and 18αGA on dispersed SMC

Membrane properties	*18βGA (30 μM)*			*18αGA (30 μM)*		
	Control	*In treatment*	*Change*	*Control*	*In treatment*	*Change*
Input resistance near −40 mV (MΩ)	2950±345	2428±313* ($n=8$)	−525±184* (−17.8%)	2650±295	3200±295* ($n=8$)	550±204* (+20.8%)
Resting potential (mV)	−21.6±2.84	−17.1±2.66* ($n=7$)	4.57±1.42*	−19.2±1.58	−17.1±1.1* ($n=10$)	2.1±1.2*
Input capacitance (pF)	7.4±0.46	7.0±0.64 ($n=5$)	−0.36±0.38	6.7±0.54	6.8±0.52 ($n=8$)	0.08±0.09

*$P<0.05$, paired *t*-test.

concentration of 0.1 μM ($P<0.05$, paired *t*-test, $n=13$). Figure 5 depicts the collective data from 13 to 16 cells where the G_{in} was measured in increasing concentrations (0.1, 1, 3, 10, 30 and 100 μM) of 18βGA.

18αGA exerted a similar but weaker gap junction blockade than 18βGA when tested with the same protocol (Figure 5 and Table 1). 18αGA at 30 and 100 μM caused a conductance reduction of ~60% (Table 1) and 67±2.4% ($n=11$), respectively, which is a significantly weaker inhibition than that by 18βGA ($P<0.05$), and the voltage step-induced current transient remained a multi-term exponential. Its IC_{50} (4.4 μM) was significantly greater than that for 18βGA inhibition of G_{in} ($P<0.05$). The residual conductance was 23% of the control (2.1±0.39 nS or 476±88.4 MΩ), that is, it would never achieve a complete electrical isolation of the recorded VSMC even if the highest concentration were used. The non-junctional action of 18αGA on dispersed VSMCs (Table 3) included a 21% increase in R_{in} near the HP, rather than a decrease by 18βGA, which implies that the *in situ* R_{in} change is an overestimate of the gap junction blocking efficacy of 18αGA. Besides, the 18αGA-induced net current also had an approximately linear *I*/*V* relation of a negative slope but with a reversal potential 11.4±1.2 mV more negative than the pre-drug RP ($P<0.001$, $n=24$, not shown).

Electrical transmission of acetylcholine-induced EDHF and the blockade by GAs

Acetylcholine (3 μM) induced an outward current in the majority of the *in situ* VSMCs recorded (52 of 69, Figure 6). The induced current was usually composed of two outward waveform phases: the first one often had a fast onset, peaked in a few seconds (98±9.6 pA, $n=25$), then declined and often oscillated quickly into a notch; the second one arose after the notch, and formed a dome or plateau (83±9.1 pA, $n=25$) during the acetylcholine application (Figures 6A and 7a, b). The amplitude and time course of the first fast peak were often variable in repeated acetylcholine applications in the same cell, so quantitative analysis was done only on the later slow phase.

We applied a ramp voltage command (−120 to 40 mV) before acetylcholine application, during the second waveform and after washout to construct the whole-cell *I*/*V* curves (Figure 6A and B). Subtracting the control *I*/*V* curve

from that constructed during the acetylcholine response waveform resulted in *I/V* curve of acetylcholine-induced net current (Figure 6C). The latter showed an increased conductance (positive slope) in the voltage range between −120 and −20 mV and a reversal potential of −83±2.1 mV ($n=11$), close to the calculated E_K (−85 mV). In the *I/V* curve of acetylcholine-induced net current, in addition to a positive slope between −110 and −20 mV, the *I/V* turned to a negative slope upon further depolarization, possibly owing to reduction of the driving force for Ca^{2+} influx (Ledoux *et al*., 2006). We saw this declining trend in the majority of cases (9 of 11).

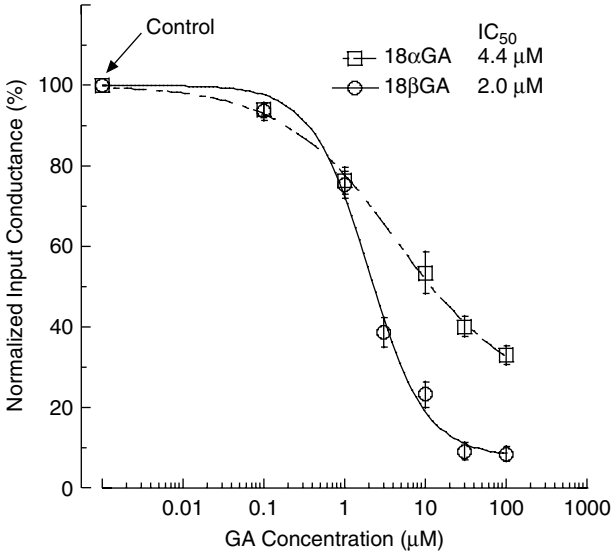

Figure 5 Concentration-dependent inhibition of GAs on membrane input conductance. Data points were from 9 to 16 cells. The curve was a least-squares fit to the means of normalized input conductance of individual cells, using the modified Hill equation: $Y=(100-C)/(1+(x/K_i)^h)+C$. For 18$\alpha$GA, the control mean input conductance (100%) was 9.1±2.2 nS ($n=14$); $IC_{50}=K_i=$ 4.4±1.1 μM; Hill coefficient $h=0.61$, and the residual conductance $C=23\pm4.3$%. For 18βGA, the control mean input conductance (100%) was 7.0±0.79 nS ($n=16$); $IC_{50}=2.0\pm0.27$ μM; Hill coefficient $h=1.2$, and the residual conductance $C=7.8\pm3.5$%. Note that in the case of 18βGA, the residual conductance 7.8±3.5% or ~0.42 nS was very close to the actual measurements at both 30 μM (9.1%, ~0.47 nS) and 100 μM (8.5%, ~0.45 nS) ($P>0.05$ in both cases). The effects of 30 and 100 μM 18βGA were not statistically different ($P>0.05$, Student's *t*-test).

Application of 18βGA (30 μM) suppressed the amplitude of acetylcholine-induced outward current by 92±2.0% ($P<0.01$, $n=10$; Figure 7), which is indicative of a strong block of myoendothelial coupling and an endothelial origin of the current (Jiang *et al*., 2005; and see Discussion section). The inhibitory effect was partially (30–80%) reversible with a wash of 18βGA-free solution for 7–10 min, and was concentration dependent with an IC_{50} of 4.3±0.19 μM (Figure 7). The IC_{50} was significantly greater than that (2.0 μM) of 18βGA inhibition on the input conductance (see above Figure 5, $P<0.001$, Student's *t*-test).

The suppression of 18αGA on the acetylcholine-induced current was also weaker than that of 18βGA (Figure 7). Unlike 18βGA, up to 1 μM 18αGA showed no significant inhibition on the acetylcholine-induced current, and 30 μM 18αGA only suppressed the current by 49.6±4.1% ($n=11$). Its IC_{50} (7.8±1.4 μM) is significantly higher than that of 18βGA ($P<0.01$, Student's *t*-test). A residual current as big as 44.7±3.8% indicates that 18αGA could not completely suppress the acetylcholine-induced current in the VSMC even at its highest concentration.

The non-junctional effects of GAs: a further study on dissociated VSMCs

As in conventional intracellular recording (Jiang *et al*., 2005), in the current clamp of *in situ* cells with whole-cell configuration, 30 μM 18βGA caused about 10 mV depolariza-

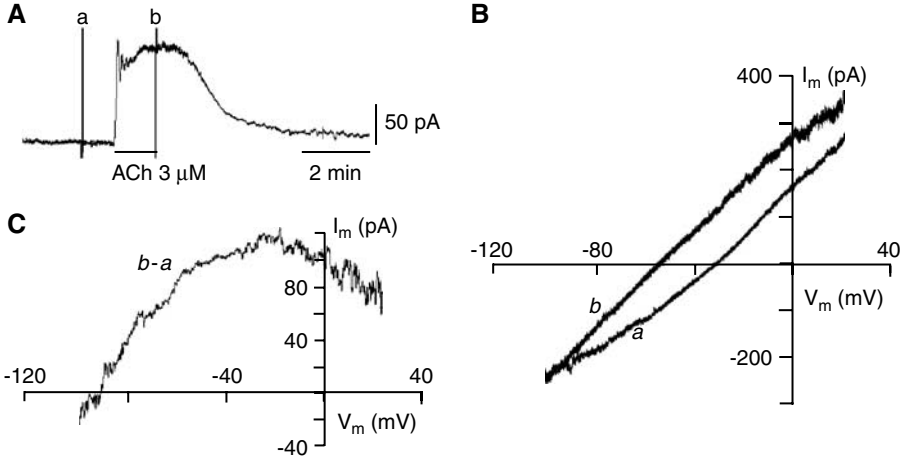

Figure 6 Acetylcholine-induced current recorded from an *in situ* VSMC. (**A**) Representative trace of acetylcholine-induced outward current, which was composed of a fast peak followed by a slow waveform. The two deflections *(a* and *b)* were whole-cell currents caused by ramp voltage commands applied before *(a)* and during *(b)* the acetylcholine-induced outward current. (**B**) *I/V* curves *(a* and *b)* constructed by the ramp commands at (*a* and *b*) in (**A**). (**C**) *I/V* relation of the acetylcholine-induced net current *(b–a)*, which had largely a positive slope with a reversal potential at −85 mV (after correction for R_a). Note that, when the clamping voltage was more positive than −20 mV, the *I/V* curve had a negative slope in this case.

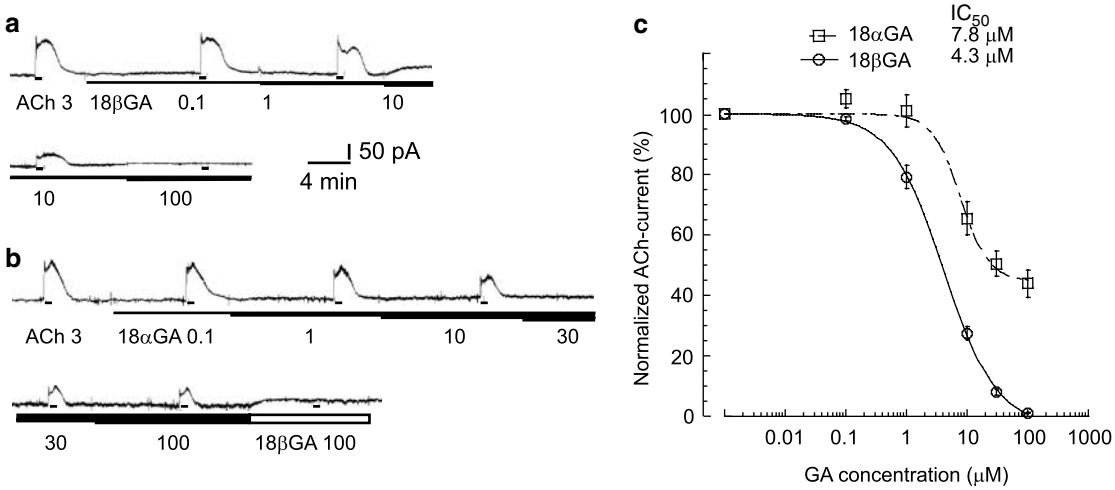

Figure 7 Concentration-dependent blockade of acetylcholine-induced outward current by GAs. (**a**) Continuous chart recording showing that 18βGA caused concentration-dependent inhibition of the 3 μM acetylcholine-induced outward current. The concentrations used (in μM) are indicated by the underline bar and numbers. (**b**) Continuous chart trace shows 18αGA inhibition of the 3 μM acetylcholine-induced outward current. Note that 18αGA up to 100 μM caused incomplete inhibition of the acetylcholine-induced current, and at the end of the trace, 100 μM 18βGA was applied for comparison. The scale bars in (**a**) apply also to (**b**). (**c**) A Hill equation fit to the means of the acetylcholine-induced current (normalized) revealed an IC_{50} of 7.8 ± 1.4 μM, a residual current of 45 ± 3.8%, Hill coefficient of 1.88, for 18αGA ($r = 0.9956$, $n \geqslant 11$), but an IC_{50} of 4.3 ± 0.19 μM, a residual current near zero, Hill coefficient of 0.98 for 18βGA ($r = 0.9999$, $n = 10$).

tion in the majority of cells sampled, indicative of a non-junctional action. In a small portion of cells that had a RP more negative than -40 mV (-51 ± 2.0 mV, $n = 6$), 30 μM 18βGA caused $\sim$29 mV depolarization (to -22 ± 3.7 mV, $P < 0.01$, paired *t*-test). A concentration of 18βGA less than 10 μM caused no significant change in membrane potential ($n \geqslant 13$). 18αGA at 30 μM also caused a depolarization ($\sim$5.8 mV, Table 1). Of note, the depolarization of *in situ* cells was associated with an inward shift of the HC at -40 mV in cells with an RP more negative than or near -40 mV (Figure 3C and D); however, it was associated with an outward shift of the HC_{-40} when the cells had a RP substantially less negative than -40 mV or had a large inward HC_{-40} (Figures 3A and 7a, b). In these cases, the blocked inward HC from the surrounding cells (tens of pA) overwhelmed the non-junctional depolarizing inward current (a few pA, Figures 8 and 9) of the isolated *in situ* cell. We further investigated the membrane channel mechanism(s) of this non-junctional depolarizing action on dissociated smooth muscle cells and described below. Application of 30 μM 18βGA caused a small but statistically significant depolarization ($\sim$4.6 mV, Table 3 and Figure 8C), or an inward HC_{-40} change (2.1 ± 0.91 pA at -40 mV, $n = 15$, Figure 8A) and a decrease in R_{in} ($\sim$525 MΩ, Table 3), but induced no significant change in input capacitance of the SMA cells. The step command-induced currents revealed that 30 μM 18βGA caused a partially reversible suppression of the leak-subtracted K_{DR} by 59 ± 5.6% at 20 mV ($n = 10$, $P < 0.05$) in all the cells tested (Figure 8B). The inhibition was similar to that of TEA but different from that of 4AP (Figure 4): effective on both fast and slow components. In the presence of 10 mM TEA, 18βGA caused only 15 ± 2.9% inhibition of the residual K_{DR} at $+20$ mV ($P < 0.01$). In contrast, the inhibition was 54 ± 3.7% in the presence of 1 mM 4AP.

In 6 of 12 cells, 18βGA also induced a net inward current between -140 and -40 mV, with approximately linear *I*/*V* relation with a positive slope of 154 ± 50 pS (Figure 8B–D), but caused no current in the remaining cells in this voltage range (not shown). The fitted line extrapolated to a reversal potential of -12 ± 4.4 mV (ranged from -5 to -20 mV, $n = 5$), suggesting activation of a non-selective cation conductance.

Application of 30 μM 18αGA caused a 2.1 mV depolarization of the dissociated cells and increased the input resistance (Table 3 and Figure 9). The *I*/*V* relationship of 18αGA-induced net current showed a K_{DR} inhibition in the majority of cells tested (6 of 7; Figure 9), similar to that by 18βGA (Figure 8B); whereas it had a negative slope *I*/*V* segment (-131 ± 11 pS) between -140 and -40 mV with a reversal potential -91 ± 6.6 mV ($n = 4$ of 6; Figure 9), suggesting inactivation of a K^+ channel.

Discussion

The tight-seal whole-cell/patch clamp recording technique is a powerful method and has become widely used in almost all fields of modern biomedical research since its invention in 1976 (Neher and Sakmann, 1976; Neher *et al*., 1978; Hille, 2001). This report is the first demonstration of its application in smooth muscle cells embedded in a segment of inner ear arteriole. It is also among the few reports showing successful whole-cell recording from cells in an intact small artery or arteriole (Quinn and Beech, 1998; Yamamoto *et al*., 1998, 2001; Guibert and Beech, 1999; Quinn *et al*., 2000; Yamazaki and Kitamura, 2001).

Our study not only extended the previous observations of 18βGA and 18αGA actions on gap junctions regarding their efficacy and gap junction-type selectivity, but also analyzed their non-junctional membrane actions on the VSMC *in situ* and in dissociated status. First, 18βGA concentration-dependently blocked the gap junction coupling of *in situ* VSMCs in the SMA with an IC_{50} of 2.0 μM. 18αGA was much less potent

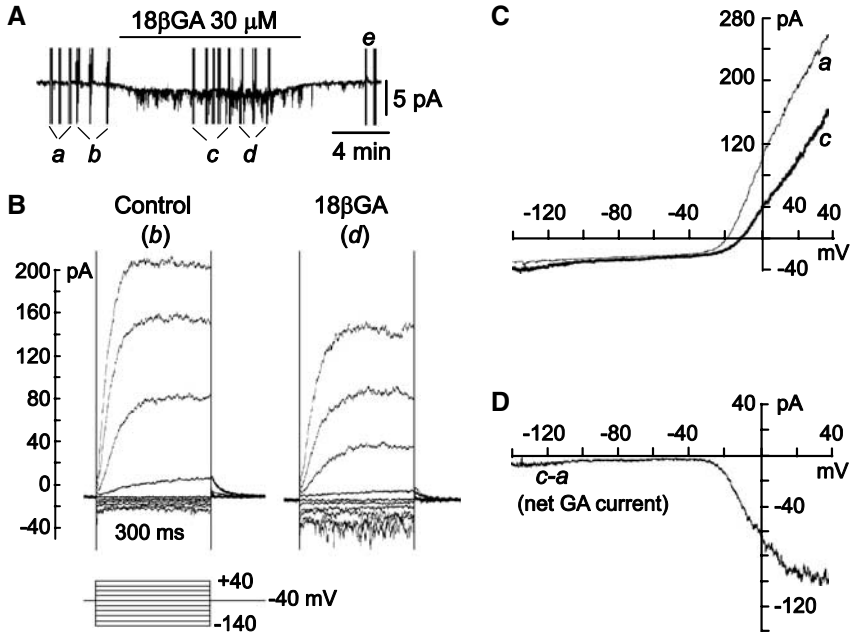

Figure 8 18βGA caused inhibition of the delayed rectifier K^+ channels in a dissociated VSMC of the SMA. (**A**) The gap-free trace depicts that 18βGA produced a reversible oscillatory inward current at HP −40 mV. The vertical deflections were truncated traces caused by repeated ramp *(a, c* and *e)* and step *(b* and *d)* voltage commands (−140 to 40 mV). (**B**) Step command-induced currents taken at (*b* and *d*) in **(A)**, showing that the delayed outward rectifier current was inhibited by 18βGA, whereas currents evoked by hyperpolarizing steps were slightly enhanced. (**C**) The ramp-constructed *I/V* curves of the whole-cell current in the presence *(c)* and absence *(a)* of 18βGA, show the same results as in **(B)**. Traces in (**B** and **C**) were from averaging 3–5 repeats of commands. (**D**) 18βGA-induced net current obtained by subtracting the control *I/V* curve (a) from that in the presence of 18βGA *(c)*. Additionally, the 5 min washout made a full recovery of the HC but the K_{DR} recovery (*e, I/V* plot not shown) from 18βGA inhibition was partial.

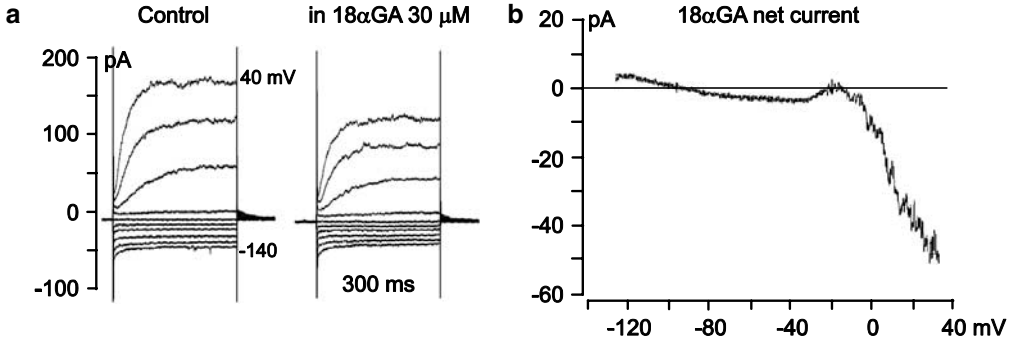

Figure 9 18αGA exerts non-junctional membrane actions partially different from those of 18βGA. Data of a representative cell (**a** and **b**) were obtained by the same protocol as shown in Figure 8. The gap-free recording is not shown. Note that 18αGA caused an inhibition of outward rectification (**a**, also **b**: a steep negative slope *I/V* between −20 and 40 mV in this case), and it also reduced the slope conductance between −140 and −40 mV (**a**). The net current *I/V* in this voltage range showed a shallow negative slope with a reversal potential near calculated E_K (−85 mV).

than 18βGA. Second, we found that the IC_{50} in blocking the myoendothelial coupling was at least twofold (4.3 μM) that for G_{in} blockage (see below for further discussion). Third, we demonstrated that it is feasible to realize an electrical isolation of arteriolar VSMC by 18βGA, instead of by dispersion; the latter inevitably introduces greater chemical and mechanical damage to the cells. The reversibility of such chemical isolation offers unique opportunity to study the role of gap junctions in intercellular communication, such as the EDHF. Finally, we demonstrated for the first time that the non-junctional membrane actions of the GAs commonly involve an inhibition of voltage-dependent K_{DR} channels, whereas 18βGA also activates a non-selective cation conductance and 18αGA inhibits a voltage-independent K^+ conductance.

Conservation of vascular physiological property

It has been shown recently that VSMCs and ECs influence each other as a functional unit and that the ECs rely on the smooth muscle cells for their intracellular ionic composition and RP (Yamamoto and Suzuki, 2005). Therefore, it is

particularly important for a study to use *in situ* vascular cells to determine the cellular and intercellular physiological mechanisms. Our data showed that the VSMCs embedded in the enzyme-treated SMA segment largely conserved the main electrophysiological properties of the vessel.

First, our data showed that K_{DR} (K_V and BK_{Ca}) channels were well preserved in cells of the enzyme-treated vessel segment and even in dissociated VSMCs (Figures 3, 4, 8 and 9). The large variation of the RP among the *in situ* cells also indicated that the K_{ir}-dependent bimodal RP feature (−40 vs −75 mV, see Jiang *et al*., 2001) of the SMA cells was retained in the vessel segment to a degree, which also explained the large variation of HC_{-40} in the absence of the GA. In this respect, however, we never saw a cell that had a RP more negative than −63 mV in this whole-cell recording study, in contrast to the conventional intracellular recording where about half of the cells had a RP near −75 mV due to the maximally activated K_{ir} (Jiang *et al*., 2001). The dialysis of the cell content could be partially responsible for the difference between the RPs measured by this whole-cell recording and our previous intracellular recording. The even poorer conservation of K_{ir} in dispersed cells may be owing to a full dialysis of the cell content in addition to the dissociation. A modification of the internal solution remains to be tested as a means of preserving the K_{ir} more effectively.

Second, the gap junction-mediated electrical coupling with surrounding cells was conserved in the vessel preparation. This is supported by our data: before GA application: (1) the input resistance was ∼200 MΩ, which was much lower than that of the dispersed single VSMC (∼3 GΩ, Table 2; also 3–5 GΩ by Gelband and Hume, 1992; Wang and Mathers, 1993); (2) the current traces during voltage steps showed a multiple term exponential decay (Figure 2d), in contrast to the single exponential decay always observed in dispersed VSMCs; (3) an endothelium-dependent acetylcholine-induced current could be recorded in the VSMC (Figures 6 and 7). These data are consistent with those by Yamamoto *et al*. (1998, 1999, 2001) who used a similar method, but contrast with a report that HEPES buffer suppressed arterial gap junction communication (Edwards *et al*., 2001) (Supplementary Figure S3). The reason for such a difference is not fully understood at the moment, but it may be owing to prolonged incubation (16–22 h) in HEPES buffer in the earlier study (Edwards *et al*., 2001).

Gap junction blocking actions of 18βGA and 18αGA

The effect of blocking gap junction coupling by 18βGA (30 μM) was first indicated by an increase in R_{in} to ∼2.2 GΩ or a 91% decrease in G_{in} of *in situ* cells (Figures 2, 3 and 5). As mentioned above in Results section, 30 μM 18βGA induced a 17.8% decrease in the R_{in} of dispersed VSMCs (Table 2). Without such non-junctional R_{in} reduction, 30 μM 18βGA would have induced a R_{in} of about 2.67 GΩ in the recorded cell. Together with an *in situ* C_{in} of ∼12 pF, the values are comparable to those of freshly dispersed single VSMCs from the SMA (∼3.0 GΩ and ∼6.1 pF; Table 2). The differences were expected since the dispersion almost always nipped off the long processes of VSMCs and made the VSMC rounder, which would increase R_{in} and decrease C_{in}. Second, the single exponential decay of a voltage step-induced current in 18βGA (Figure 2e) indicates a single RC circuit load, suggesting full electrical isolation of the recorded cell *in situ* (Lindau and Neher, 1988; de Roos *et al*., 1996). Our data support the notion that 18βGA at or above 30 μM achieves an almost full electrical isolation.

The concentration–response curve indicated that 18βGA had an IC_{50} of 2.0 μM for blocking the VSMC electrical coupling, which is equal to the value (2 μM) from a metabolic co-operation assay on human fibroblast intercellular junction communication (Davidson and Baumgarten, 1988). This consistency may either reflect a similar molecular structure between the gap junctions of blood vessels and human fibroblasts cells, as both contain connexins 43 and 45 (Figueroa *et al*., 2004; Kohl *et al*., 2005), or that this compound exhibits little specificity for the various types of connexin. However, our data suggested otherwise because it took at least twofold higher concentrations to block the myoendothelial gap junction-mediated acetylcholine response than blocking the intramuscular coupling (Figure 7).

In contrast to previous reports that 18αGA had no significant effect on gap junction communication (Coleman *et al*., 2001; Matchkov *et al*., 2004), we were able to demonstrate its gap junction blocking effect (Figures 5 and 7). However, this action was significantly weaker than that of 18βGA in two aspects: the IC_{50} of 18αGA was over twofold higher and the maximal conductance attenuation was 15% less than that of 18βGA. The differences would be even greater when the opposite actions of the two compounds on R_{in} of dispersed cells are taken into consideration.

Electrical and chemical transmission of acetylcholine-induced EDHF

This study demonstrates that 30 μM 18βGA blocked the acetylcholine-induced electrical response by 92%, which is obviously higher than the 84.6% observed with intracellular experiments (Jiang *et al*., 2001). At present, we do not fully understand what caused this discrepancy, but one possible explanation is as follows. When the VSMC was voltage-clamped at −40 mV, K_{ir} was kept inactivated and no regenerative hyperpolarization was permitted; this would otherwise have generated 35% of the aceylcholine hyperpolarization in intracellular recordings (Jiang *et al*., 2005). Moreover, the complete inhibition of the acetylcholine-induced current by 100 μM 18βGA may not be fully explained by a gap junction blockade, if the K^+-release pathway remains intact (Jiang *et al*., 2005); instead, it suggests that the GA may have a non-junctional action which directly inhibits the acetylcholine-induced K_{Ca} activation in the ECs, as suggested previously (Coleman *et al*., 2001). The dissociated VSMC data indicated an inhibition by the GAs of K_{DR}, including the BK_{Ca} (Figures 8 and 9), which raises the possibility that the GAs could also suppress the intermediate conductance K_{Ca} channel (IK) activation in the ECs by interfering with Ca^{2+} influx or release from the Ca^{2+} store. More experiments are needed to test this possibility.

Our IC_{50} data appear to suggest that myoendothelial coupling is twofold less sensitive than VSMC–VSMC coupling to 18βGA, but this difference could be somewhat

underestimated. The higher IC_{50} for blocking acetylcholine-induced current means that the harder-to-block myoendothelial coupling may have compromised the G_{in} suppression, thus increasing the IC_{50} value for G_{in}. However, this increase might be minimal. First, our previous study demonstrated that myoendothelial coupling is weak and/or not every VSMC contacts ECs (Jiang *et al*., 2001, 2005). Second, as shown in Figures 2 and 3, 30 μM 18βGA, a concentration that is less than 10-fold higher than the IC_{50} for acetylcholine-induced current inhibition actually caused a full electrical isolation – the residual myoendothelial coupling was undetectable. Moreover, GA effects on the acetylcholine-induced outward current could be studied only in VSMCs (52 of 69) that had direct or indirect electrical coupling with ECs. The acetylcholine-induced current in the VSMCs that had only indirect communication with ECs would be suppressed when the VSMC–VSMC coupling was blocked. This should have resulted in lowering the IC_{50} of GA for acetylcholine-induced current inhibition.

Non-junctional membrane action of the GAs

Our data suggest that the ionic mechanism of non-junctional action of both the GAs on the VSMC involved two conductance changes. In dissociated VSMCs, 18βGA (30 μM) induced a current that had I/V relation with two apparent segments: a positive slope (increase in G_{in}) on the left and a negative slope (decrease in G_{in}) on the right of ~ -40 mV (Figure 8). The negative slope segment was consistent with an inhibition of the BK_{Ca} and K_V (or K_{DR}, Figure 8; Hille, 2001), which would cause a depolarization in cells that had a low RP. The BK_{Ca} inhibition is consistent with an I_{Ca} inhibition by 18βGA in the VSMC reported previously (Matchkov *et al*., 2004). The positive slope segment and the decrease in R_{in} (Table 2) are consistent with an activation of a non-selective cation conductance. This 18βGA-activated conductance is expected to cause a strong depolarization when the cell had a highly negative RP owing to a big driving force. This depolarization could de-activate the K_{ir} in these cells, which would cause an amplification of the depolarization. These mechanisms could explain why 18βGA caused a bigger depolarization in high RP cells in the present study and the study by others (Coleman *et al*., 2001).

The inhibition of K_{DR} by 18αGA seems similar to that induced by 18βGA. However, in a voltage range between -140 and -40 mV, 18αGA caused a net current associated with a decrease in slope conductance and reversed at ~ -91 mV, suggesting an inactivation of K^+ conductance. The nature of this K^+ conductance remains to be identified although its linear I/V over a wide voltage range would correspond to several K^+ channels that are active in physiological background conditions and are only slightly sensitive to voltage (Jackson, 2005).

Taken together, our findings of the junctional and non-junctional membrane actions of the GAs are different in many aspects from previous reports (Coleman *et al*., 2001; Matchkov *et al*., 2004). Among several possible reasons for such a discrepancy – the animal species, the vascular bed, the size of the vessel and the recording method – we believe the last two are the most relevant here. It is generally recognized that the input resistance measurement with sharp electrode recording is often unreliable because the high-resistance electrode may change its resistance, especially when a current command is applied, and the bridge circuit is difficult to keep perfectly balanced (Purves, 1981). The thinner vessel and the enzyme digestion currently used may have facilitated the diffusion of the compound to its sites of action.

In summary, our data demonstrated a reasonable conservation of membrane properties in the enzyme-cleaned vessel, which validates the usefulness of this *in vitro* preparation for whole-cell recording study of the interaction between endothelial and muscular layers. Moreover, our finding that 30 μM 18βGA almost fully isolated the *in situ* VSMCs with mild non-junctional actions near physiological resting potential offers an opportunity for voltage-clamp investigation of the ion channels in cells under non-dispersed condition. This approach could be particularly valuable for arterioles such as the inner ear artery where the channel mechanisms are little known.

Acknowledgements

This work was supported by NIH NIDCD DC 004716 and NIH P30 DC005983. We also thank Electra Allenton and Jill Lilly for their reading of the manuscript.

Conflict of interest

The authors state no conflict of interest.

References

Armstrong CM, Gilly WF (1992). Access resistance and space clamp problems associated with whole-cell patch clamping. *Methods Enzymol* **207**: 100–122.

Bradley KK, Jaggar JH, Bonev AD, Heppner TJ, Flynn ER, Nelson MT *et al*. (1999). Kir2.1 encodes the inward rectifier potassium channel in rat arterial smooth muscle cells. *J Physiol (Lond)* **515**: 639–651.

Busse R, Edwards G, Feletou M, Fleming I, Vanhoutte PM, Weston AH (2002). EDHF: bringing the concepts together. *Trends Pharmacol Sci* **23**: 374–380.

Coleman HA, Tare M, Parkington HC (2001). K^+ currents underlying the action of endothelium-derived hyperpolarizing factor in guinea-pig, rat and human blood vessels. *J Physiol* **531**: 359–373.

Davidson JS, Baumgarten IM (1988). Glycyrrhetinic acid derivatives: a novel class of inhibitors of gap-junctional intercellular communication. Structure–activity relationships. *J Pharmacol Exp Ther* **246**: 1104–1107.

de Roos AD, van Zoelen EJ, Theuvenet AP (1996). Determination of gap junctional intercellular communication by capacitance measurements. *Pflugers Arch* **431**: 556–563.

Edwards G, Feletou M, Gardener MJ, Glen CD, Richards GR, Vanhoutte PM *et al*. (2001). Further investigations into the endothelium-dependent hyperpolarizing effects of bradykinin and substance P in porcine coronary artery. *Br J Pharmacol* **133**: 1145–1153.

Figueroa XF, Isakson BE, Duling BR (2004). Connexins: gaps in our knowledge of vascular function. *Physiology (Bethesda)* **19**: 277–284.

Gelband CH, Hume JR (1992). Ionic currents in single smooth muscle cells of the canine renal artery. *Circ Res* **71**: 745–758.

Griffith TM (2004). Endothelium-dependent smooth muscle hyperpolarization: do gap junctions provide a unifying hypothesis? *Br J Pharmacol* **141**: 881–903.

Guan BC, Nuttall AL, Jiang ZG (2006). Whole-cell recording of smooth muscle cells in guinea pig *in vitro* spiral modiolar artery. *Assoc Res Otolaryngol Midwin Res Meet Abstr* **29**: #604.

Guibert C, Beech DJ (1999). Positive and negative coupling of the endothelin ETA receptor to Ca^{2+}-permeable channels in rabbit cerebral cortex arterioles. *J Physiol* **514**: 843–856.

Hille B (2001). *Ionic Channels of Excitable Membranes*. Sinauer Associates Inc.: Massachusetts.

Jackson W (2005). Potassium channels in the peripheral microcirculation. *Microcirculation* **12**: 113–127.

Jiang ZG, Nuttall AL, Zhao H, Dai CF, Guan BC, Si JQ *et al.* (2005). Electrical coupling and release of K^+ from endothelial cells comediate ACh-induced smooth muscle hyperpolarization in guinea-pig inner ear artery. *J Physiol* **564**: 475–487.

Jiang ZG, Si JQ, Lasarev MR, Nuttall AL (2001). Two resting potential levels regulated by inward rectifying potassium channels in guinea pig cochlea spiral modiolar artery. *J Physiol (Lond)* **537**: 829–842.

Kikuchi T, Adams JC, Miyabe Y, So E, Kobayashi T (2000). Potassium ion recycling pathway via gap junction systems in the mammalian cochlea and its interruption in hereditary nonsyndromic deafness. *Med Electron Microsc* **33**: 51–56.

Kohl P, Camelliti P, Burton FL, Smith GL (2005). Electrical coupling of fibroblasts and myocytes: relevance for cardiac propagation. *J Electrocardiol* **38**: 45–50.

Ledoux J, Werner ME, Brayden JE, Nelson MT (2006). Calcium-activated potassium channels and the regulation of vascular tone. *Physiology (Bethesda)* **21**: 69–78.

Lindau M, Neher E (1988). Patch-clamp techniques for time-resolved capacitance measurements in single cells. *Pflugers Arch* **411**: 137–146.

Matchkov VV, Rahman A, Peng H, Nilsson H, Aalkjaer C (2004). Junctional and nonjunctional effects of heptanol and glycyrrhetinic acid derivates in rat mesenteric small arteries. *Br J Pharmacol* **142**: 961–972.

Neher E, Sakmann B (1976). Single-channel currents recorded from membrane of denervated frog muscle fibres. *Nature* **260**: 799–802.

Neher E, Sakmann B, Steinbach JH (1978). The extracellular patch clamp: a method for resolving currents through individual open channels in biological membranes. *Pflugers Arch* **375**: 219–228.

Palmada M, Schmalisch K, Bohmer C, Schug N, Pfister M, Lang F *et al.* (2006). Loss of function mutations of the GJB2 gene detected in patients with DFNB1-associated hearing impairment. *Neurobiol Dis* **22**: 112–118.

Purves RD (1981). *Microelectrode Methods for Intracellular Recording and Ionophoresis*. Academic Press Inc.: New York.

Quinn K, Beech DJ (1998). A method for direct patch-clamp recording from smooth muscle cells embedded in functional brain microvessels. *Pflugers Arch* **435**: 564–569.

Quinn K, Guibert C, Beech DJ (2000). Sodium-potassium-ATPase electrogenicity in cerebral precapillary arterioles. *Am J Physiol Heart Circ Physiol* **279**: H351–H360.

Sabag AD, Dagan O, Avraham KB (2005). Connexins in hearing loss: a comprehensive overview. *J Basic Clin Physiol Pharmacol* **16**: 101–116.

Sandow SL (2004). Factors, fiction and endothelium-derived hyperpolarizing factor. *Clin Exp Pharmacol Physiol* **31**: 563–570.

Segal S (2005). Regulation of blood flow in the microcirculation. *Microcirculation* **12**: 33–45.

Wang Y, Mathers DA (1993). Ca^{2+}-dependent K^+ channels of high conductance in smooth muscle cells isolated from rat cerebral arteries. *J Physiol (Lond)* **462**: 529–545.

Yamamoto Y, Fukuta H, Nakahira Y, Suzuki H (1998). Blockade by 18beta-glycyrrhetinic acid of intercellular electrical coupling in guinea-pig arterioles. *J Physiol (Lond)* **511**: 501–508.

Yamamoto Y, Imaeda K, Suzuki H (1999). Endothelium-dependent hyperpolarization and intercellular electrical coupling in guinea-pig mesenteric arterioles. *J Physiol (Lond)* **514**: 505–513.

Yamamoto Y, Klemm MF, Edwards FR, Suzuki H (2001). Intercellular electrical communication among smooth muscle and endothelial cells in guinea-pig mesenteric arterioles. *J Physiol* **535**: 181–195.

Yamamoto Y, Suzuki H (2005). Dependency of endothelial cell function on vascular smooth muscle cells in guinea-pig mesenteric arteries and arterioles. *J Smooth Muscle Res* **41**: 77–85.

Yamazaki J, Kitamura K (2001). Cell-to-cell communication via nitric oxide modulation of oscillatory Cl^- currents in rat intact cerebral arterioles. *J Physiol* **536**: 67–78.

Supplementary Information accompanies the paper on British Journal of Pharmacology website (http://www.nature.com/bjp)

Please note that this manuscript is a correction of an original version that was published in advance online (AOP) on 18 June 2007. Corrections have been made to the whole-cell current *I/V* plots in Figures 3C and 3D. Other minor changes have not affected the scientific content of the article.